their Fig. 6). Hodges et al. (2003) and Kerns et al. (2008) found similar results. However, an hypothesis of in situ development of waves is perhaps contrary to prevailing theories as discussed extensively in Part I. For example, Raymond et al. (2006) consider that the eastern Pacific Ocean is perturbed by the passage of waves generated remotely in the North Atlantic Ocean, presumably over West Africa. Other studies (e.g., Farfan and Zehnder 1997; Zehnder and Gall 1991; Zehnder et al. 1999) suggest that the high mountains of the Isthmus of Panama and western Mexico (Fig. 1a) are instrumental in the generation of disturbances or major perturbing factors of waves that propagate from the North Atlantic Ocean. Here we test, through controlled numerical experiments, the relative importance of easterly waves propagating from the northern Atlantic Ocean versus in situ wave development. Furthermore, experiments are performed that test the importance of elevated terrain.

The numerical model used in the experiments is described in Sect. 2. The experimental setup is provided in Sect. 3 and the results of the experiments are discussed in Sect. 4. Some conclusions are given in the final section.

2 Model description

Numerical experiments are conducted using the Weather Research and Forecasting regional model (WRF: version 2.2, Skamarock et al. 2005). The WRF is a fully compressible model and uses high-order advection schemes on an Arakawa-C grid on a terrain-following hydrostatic-pressure vertical coordinate defined as $\sigma = (p_h - p_{ht})/\mu$. Here $\mu = p_{hs} - p_{ht}$, where p_h is the hydrostatic component of the pressure and p_t and p_s represent the values at the top and surface values, respectively (Laprise 1992). The WRF incorporates the third-order Runge–Kutta time integration scheme described by Wicker and Skamarock (2002).

The model is configured with 28 vertical levels with pressure p_t set at 56 hPa and a 56 km horizontal resolution. The WRF-Single-Moment class-5 microphysics scheme (Hong et al. 2004) is chosen in addition to the long-wave radiation parameterization of Mlawer et al. (1997). The model contains the Dudhia (1989) short-wave radiation scheme, the Monin–Obukhov surface flux calculation scheme and the YSU boundary layer scheme is used (Noh et al. 2003). The Betts–Miller–Janjic scheme (Betts and Miller 1993; Janjic 1994) is chosen for the convective parameterization.

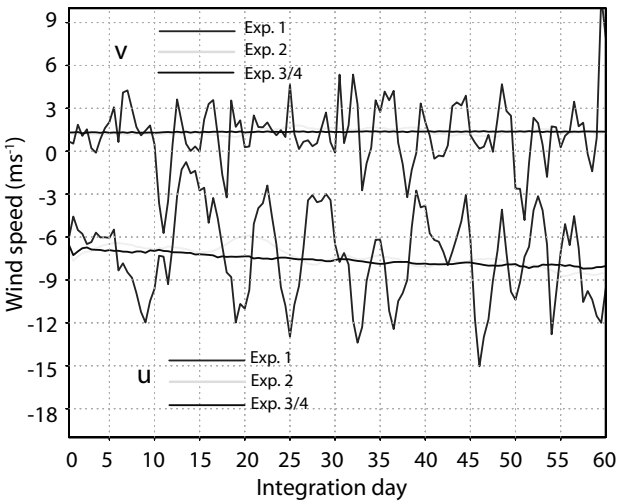

Fig. 2 Variability of the boundary conditions at a point 65W, 15 N and 700 hPa for the meridional and zonal velocity components. Time series for the four experiments described in Table 1 are shown. Boundary conditions were applied at all boundary points and all variables. The first 60 days of the experiments are shown. Data from ERA-40 reanalysis (Uppala et al. 2005)

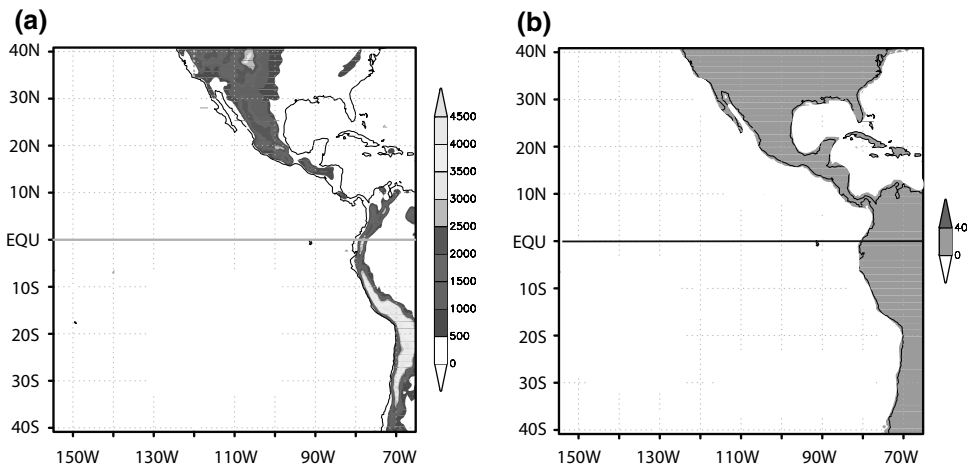

Fig. 1 a Physical domain (domain with full topography) 40 N–40 S and 65E–155W used in all WRF simulations. Terrain height (contour interval 50 m) used in Experiments 1–4. b Domain with flat topography. Terrain height for Experiment 4. Terrain is leveled at a constant 40 m

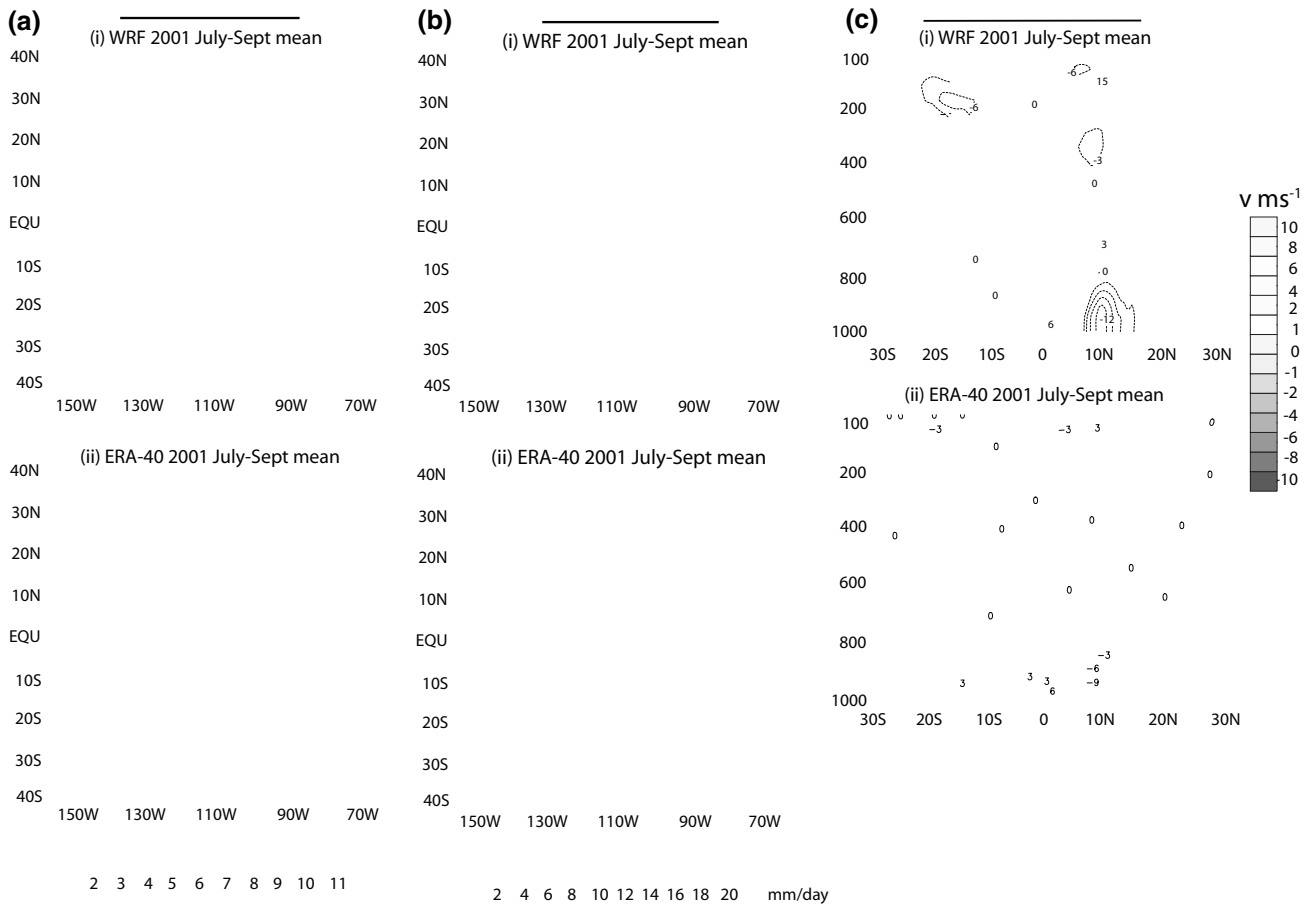

Fig. 3 a Mean distribution of the 10-m horizontal surface wind Þeld (i) days 31Ð121 of integration (units: m s^{-1}) of Experiment 1, the control integration, and (ii) the 1 JulyÐSeptember ERA40 reanalysis mean for the same period (units: m s^{-1}). The thick black line represents the mean absolute vorticity = 0 line at 10 m. WRF resolution is 56 km compared to 250 km for ERA-40. b Mean distribution of the precipitation Þeld rate (i) (days 31Ð121 of integration (units: m s^{-1}) of Experiment 1, the control integration, and (ii) the mean precipitation rates from GPCP averaged for the same period (units mm day^{-1}). WRF resolution is 56 km compared to 250 km for GPCP. c Comparison of the (i) simulated mean (days 31Ð121) and (ii) the observed long-term mean 1981Ð2000 for JulyÐSeptember in the east Paciþc Ocean averaged for 110Ð90W. In both panels, shading represents magnitude of meridional wind component relative to the bar on the right (units: m s^{-1}), solid lines show horizontal wind divergence (contour interval: $\times 3 10^{-6}$ s^{-1}, dotted lines represent negative values) and the = 0 contour (thick black line). WRF resolution is 56 km compared to 250 km for ERA-40

3 Experimental design

The experimental domain is shown in Fig. 1a and possesses latitudinal boundaries at 30S and 40N and lateral boundaries at 155W and 65W. Besides the eastern equatorial Paciþc Ocean, these boundaries include the western North Atlantic Ocean and the mountainous terrain of Mexico, Central America and western South America.

Several experiments were designed to test hypotheses put forward in Part I and those postulated elsewhere. Experiment 1 is the control case where full boundary conditions are used at domain boundaries. Thus, in Experiment 1, there exists the potential for high frequency easterly waves to enter the eastern Paciþc Ocean. Since one of the objectives of this study is to examine the relationship between the cross-equatorial lower tropospheric ßow in the eastern Paciþc and easterly waves activity, the model-simulated basic state needs to reproduce reality with some Þdelity. The results of the control case will be compared with analyses of observed mean states. Experiment 2 is identical to the control case except that a 10-day running average is applied to the boundary conditions. The aim here is to remove high frequency easterly wave forcing from the Atlantic Ocean. Experiment 3 uses an extrapolation of the mean monthly boundary conditions further eliminating variability from boundary forcing. To reduce the degrees of freedom in Experiment 3, the SST distribution was kept constant for the duration of the experiment. Finally, in Experiment 4 the orographic features are removed from the lower boundary and are replaced by a

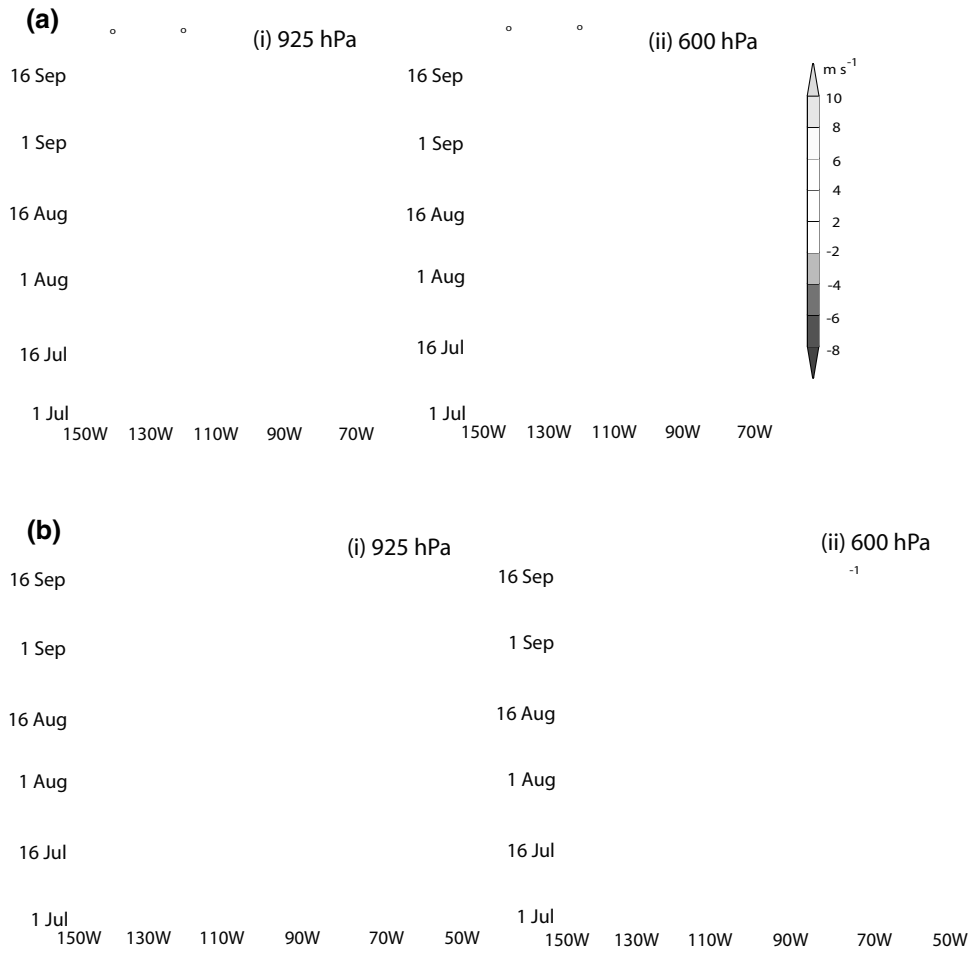

Fig. 4 a Time–longitude diagrams of the mean 925 and 600 hPa meridional wind in the band 7.5°N–12.5°N (shading relative to the bar on the right, units: m s^{-1}) for days 31–121 between 150°W and 65°W. b Same as a, except for the eastern boundary moved 15° eastward to 50°W

uniform elevation of 40 m overall land areas. The aim of this experiment is to determine if orography has a major role in perturbing the eastern Paciþc ITCZ.

The ECMWF ERA40 reanalysis data set (Uppala et al. 2005) is used as initial data and boundary conditions in all simulations. The horizontal resolution of the ERA-40 is 2.5° (downscaled to 1°) with 18 levels in the vertical. The lateral boundary conditions are updated every 6 h at all levels either with unþltered data (Experiment 1) or with various þltering (Experiments 2–4). The SST þelds in the ECMWF ERA-40 dataset are obtained from externally produced analysis from United Kingdom Meteorological Oþce and National Ocean-Atmosphere Agency SST þelds with weekly temporal resolution (Reynolds et al. 2002). Where necessary, these data are linearly interpolated to provide six hourly values.

An example of the boundary conditions at one location on the eastern boundary (65°W, 15°N) and at one level (700 hPa) is shown in Fig. 2 for the 60 days of integration. Similar boundary conditions were used in the 30-day period of spin-up. Experiment 1 expresses the full variability of the velocity þeld. Experiment 2 shows a slow modulation of the velocity þeld reßecting the 10-day running average applied at the boundary. Experiments 3 and 4 show a slow modulation from extrapolation between monthly mean values of 2 and 8 m s^{-1} for the meridional and zonal components.

It is important to emphasize that in all cases, the model is run in ÔÔfree-modeÕÕ without updating the internal domain with observations. Except for the SST þelds, which are slowly varying, and the initial and lateral boundary condition, all meteorological þelds are calculated internally within the model. All simulations are run for 121 days. The þrst 30 days are discarded to allow the model to spin-up. Given that the motivation for the numerical experiments is to determine whether or not Paciþc easterly waves develop in situ or propagate westward from the Atlantic Ocean, it is important to test the sensitivity of the model to the location of the eastern boundary. To this end, Experiment 1 (the control) is run with the boundary condition moved 15° of longitude to the east (50°W) and the experiment repeated. Also, it is important to reiterate that the boundary conditions (velocity components, geopotential, speciþc humidity, temperature) are set on all boundaries

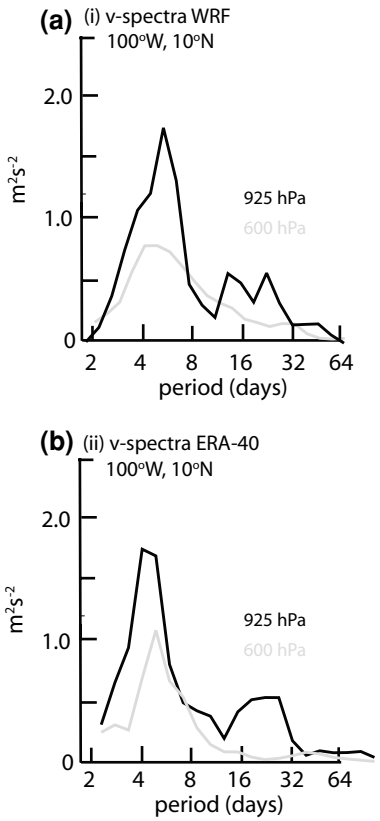

Fig. 5 Global wavelet power spectra of meridional wind at two pressure levels: 925 and 600 hPa W, 9 N. a Experiment 1 and b ERA-40 reanalysis

while precipitation is calculated internally within the WRF model. Also, ÔÔßow throughÕÕ or exponential relaxation at the boundaries were not an option in the version of the WRF available to us. Thus, quantities such as precipitation, dependent sensitively on small variations of divergence, may possess anomalous values close to the western boundary. It will be shown that these effects are small and do not effect the inner domain results and, in any case are conÞned to the western boundary that is of lesser interest to the thrust of this study.

4 Results

4.1 Control simulations

Experiment 1 is initialized at 12Z on June 1st, 2001, with lateral boundary conditions and initial conditions (geopotential height, winds, temperature, moisture and sea level pressure) updated every 6 h. Figure 3a shows the WRF simulated 10 m vector wind magnitude the model simulations averaged from day 31 to 121 (panel i) compared to ERA40 Þelds averaged over the same JulyÐSeptember period (panel ii). The thick black line represents the 10 m zero absolute vorticity isopleth $\eta (= 0)$. Although the overall surface cross-equatorial ßow pattern produced by the model is similar to the reanalysis Þelds, the magnitude of the winds is generally stronger in the simulations compared to the climatology probably due to the higher resolution of the WRF model (56 km) compared to ERA-40 (250 km).

Figure 3b shows the distribution of precipitation for Experiment 1 and the mean JulyÐSeptember GPCP precipitation for the same period. Precipitation estimates from the long-term mean Global Precipitation Climatology Project (GPCP: Adler et al. 2003) averaged between 1981 and 2000 for the JulyÐSeptember period are used to depict the observed Þelds. Maximum ITCZ convective activity for both the WRF simulations and observations is located in the 10ÐN latitude band. The smoother observed patterns again arise from difference in resolution between the 250 km grid of the GPCP versus the 56 km grid of the WRF simulations.

The mean meridional circulations averaged across the domain are shown in Fig. 3c. The observed Þelds are the same as those shown in Part I (Fig. 4a). There is strong similarity between the two sections. Both show a deep circulation with 4Ð6 m s^{-1} southerly winds in the lower troposphere and a strong 8Ð10 m s^{-1} return ßow in the upper troposphere. The $\eta = 0$ contour bisects the divergenceÐconvergence doublet near the surface. A most striking aspect of both of the Fig. 3c sections is the existence of the shallow weaker circulation between the surface and the mid-troposphere with a southward ßow of about 2Ð3 m s^{-1} identiÞed by Toma and Webster (2008) and Zhang et al. (2004). In Part I, we suggested that this shallow circulation is a signature of an oscillating ITCZ as it cycles from an unstable to a stable state. The important point is that the WRF model also produces this shallow circulation and, as we will see later, the oscillation of the ITCZ itself. Overall, Experiment 1 produces a mean meridional circulation pattern with characteristics similar to the observed east PaciÞc MMC (Fig. 4a, Part I). However, there is a difference in magnitude between the two meridional circulations that again may be attributable to the lower resolution of the observed Þelds.

The western boundary condition issue noted in the previous section can be seen in the precipitation Þeld [Fig. 3b(i)] at the latitude of the simulated ITCZ at the far west of the domain. Anomalously high precipitation occurs at the boundary. However, with experiments repeated (not shown) with the boundary moved 10 to the west (i.e., to 175 W), the precipitation anomaly, still conÞned to the boundary, moves westward as well. The internal values of precipitation are identical in both experiments. Precipitation anomalies along the eastern boundary are discussed later.

Table 1 Lateral boundary conditions, SST forcing and topography schemes used in the four experiments

	Boundary conditions	Sea-surface temperature	Topography
Experiment 1	6 h	6 h	Full
Experiment 2	10-day moving average	Monthly mean	Full
Experiment 3	30-day moving average	Monthly mean	Full
Experiment 4	30-day moving average	Monthly mean	Constant 40 m

Figure 4a shows the time–longitude evolution of unfiltered meridional wind (v) averaged between 7.5 N and 12.5 N at 925 and 600 hPa levels (panels i and ii, respectively) over the domain for days 31–121. The diagrams show westward propagating disturbances characterized by high frequency oscillations of meridional wind at both levels. The wavelengths of these disturbances are approximately 2,200–2,500 km, with propagation speeds of 6–7 m s^{-1} and periods of 3–5 days. In the vicinity of the Isthmus of Panama at 12.5 N, 85–90 W, the character of the migrations changes. Very few westward propagating disturbances appear to move into the Pacific Ocean from the Atlantic. The same changes in characteristics are observed when the eastern boundary is moved eastward to 50 W (Fig. 4b). Whereas the gross nature of the oscillations stay much the same in the Pacific (both cases show similar wavelength and propagation speeds) there are differences in the details. But, if the waves in the Pacific Ocean are indeed instability waves, as suggested in Part I, then one may expect slight differences of when a particular wave is generated due to the chaotic nature of instability. But, most importantly, the choice of the location of the eastern boundary appears to have little impact on the nature of the regional oscillations in the Pacific Ocean. In addition, the narrow precipitation anomalies along the eastern boundary also move eastward with the displaced boundary (not shown).

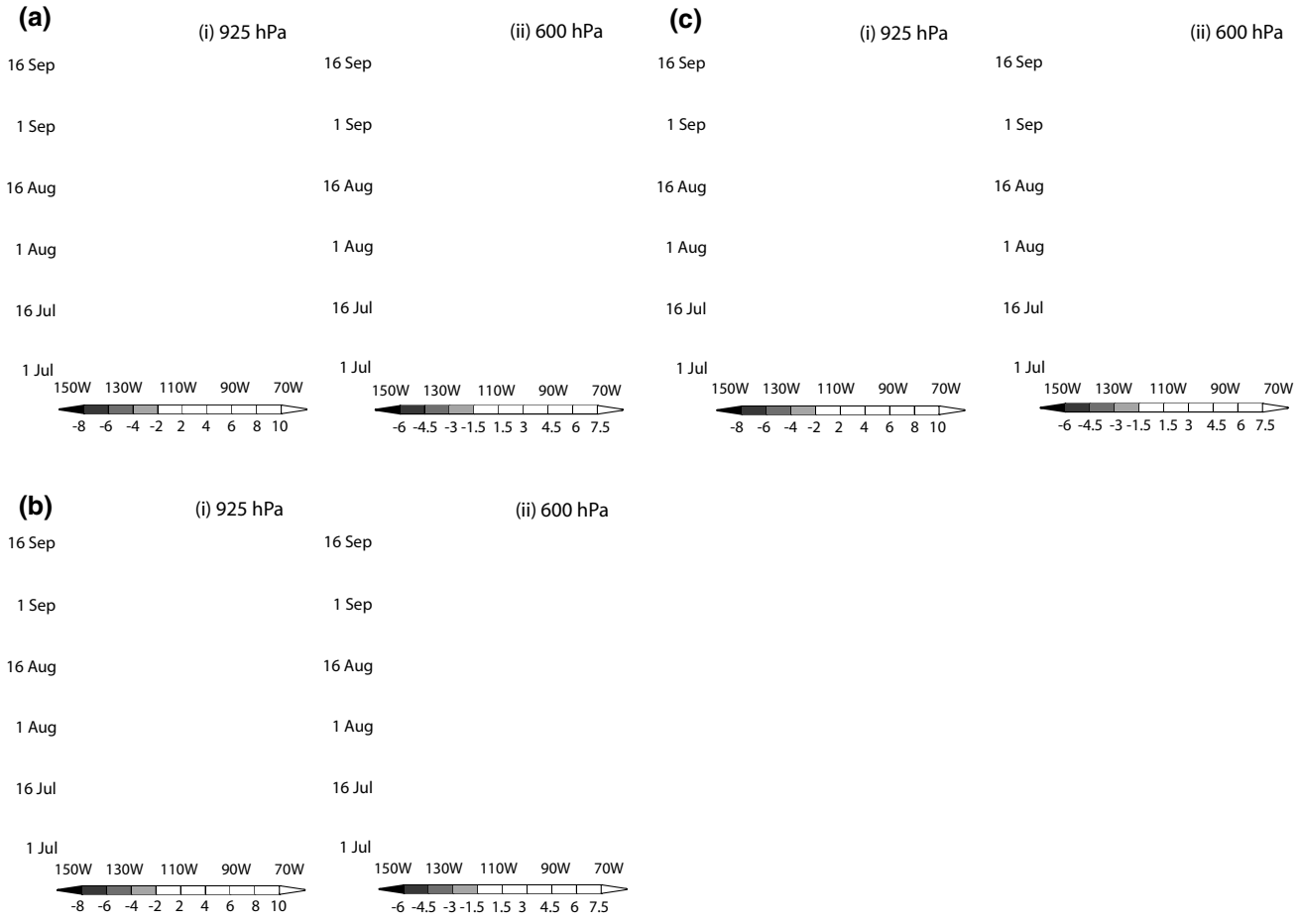

Fig. 6 Time–longitude diagrams of meridional wind (shading relative to the bar below figure, units: m s^{-1}) at 925 and 600 hPa for days 31–121 of a Experiment 2: 10-day filtered boundary conditions, b Experiment 3: monthly filtered boundry conditions and c Experiment 4: monthly filtered b.c.s and no topography. Fields are plotted between 150 W and 65 W and averaged in the 7.5 N–12.5 N band. In each figure, panel i shows the 925 hPa and panel ii 600 hPa fields

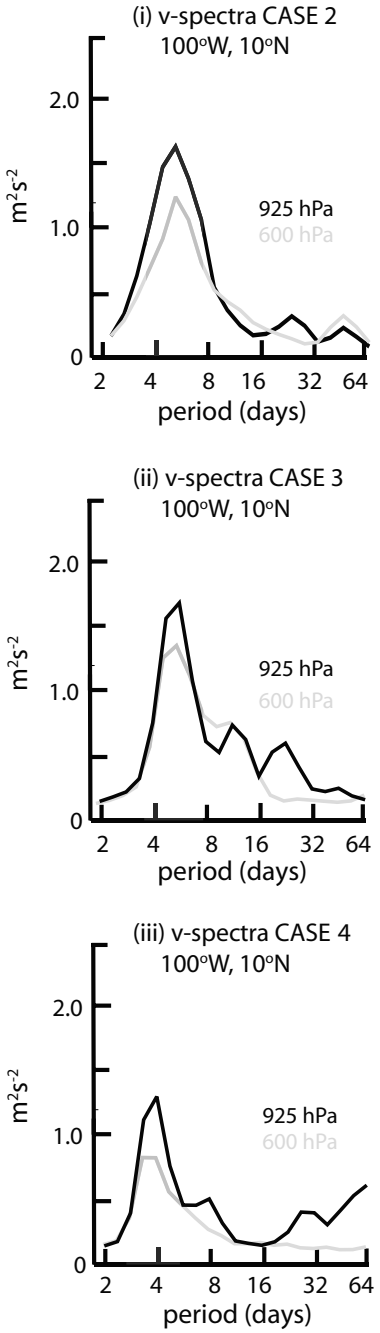

Fig. 7 Global wavelet power spectra (units: $m^2 s^{-2}$) of meridional wind at two pressure levels: 925 and 600 hPa for (i) Experiment 2, (ii) Experiment 3 and (iii) Experiment 4. All spectra are computed at (90 W; 9 N)

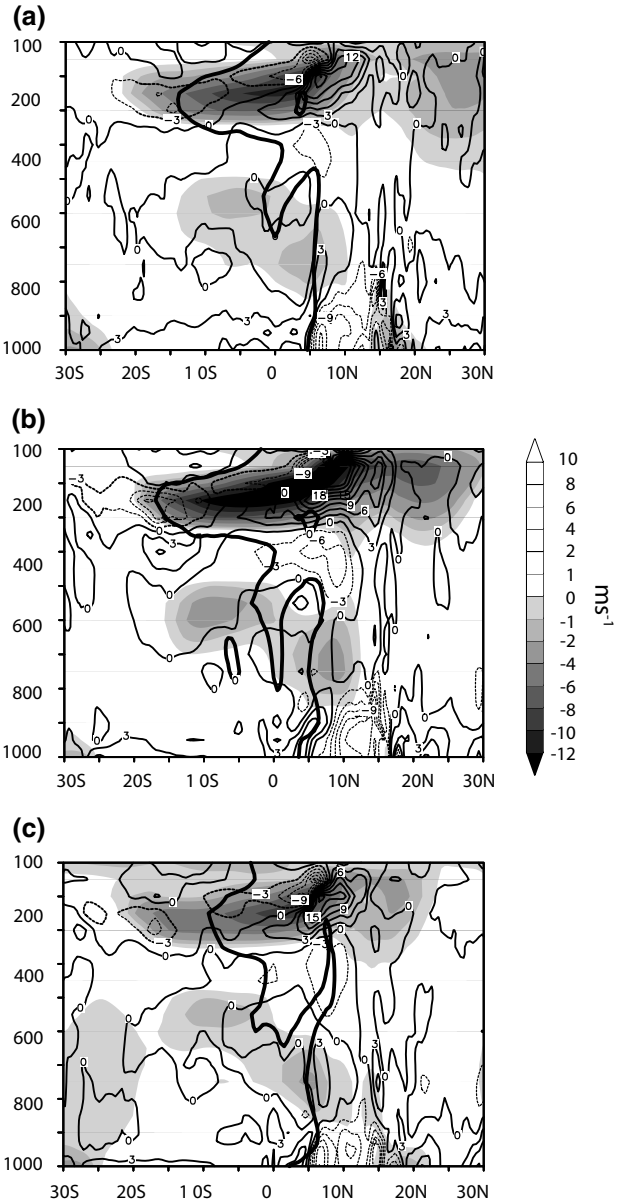

Fig. 8 Characteristics of the mean (days 31–121) simulated meridional circulation in the eastern Pacific Ocean averaged for 100–85 W for a Experiment 2: v & ∇, b Experiment 3: v & ∇ and c Experiment 4: v & ∇. Meridional wind shown as shading relative to the bar on the right, (units: m s^{-1}), horizontal wind divergence as contours (interval: 3×10^{-6} s^{-1}, dotted lines represent negative values). The heavy black line represents the $v = 0$ contour

Finally, Fig. 5 offers a quantification of the period of the disturbances showing the power spectra of meridional wind time series (days 31–121) at 925 and 600 hPa, for Experiment 1 and the corresponding power spectrum from the ERA-40 data. In both experiments, a large peak in the 4–8 day band is apparent with a strong correspondence between the observations and the model.

In summary, the control experiment shows many of the mean characteristics and similar transient behavior noted in the diagnostics described in detail in Part I. Furthermore, changing the location of the eastern boundary does not alter the character of the Pacific disturbances and errors introduced on the western boundary appear to be localized. The model appears to have sufficient similitude to be used in the series of process studies listed in Table 1.

4.2 Idealized numerical experiments

Figure 6aÐc shows the time–longitude evolution of unfiltered meridional wind (v) averaged between 7.5 N and 12.5 N at 925 hPa (left panel) and 600 hPa (right panel) over the domain for days 31–121 for the experiments summarized in Table 1. The point of comparison is Experiment 1 (Fig. 4a or b).

The first aspect of the experiments is that easterly waves of similar scale and periodicity appear in the Pacific Ocean irrespective of the eastern boundary conditions. This conclusion is supported by the very similar meridional wind spectra for each experiment at 100 W, 9 N for 925 and 600 hPa levels (Fig. 7). A broad high frequency peak in the 4–8 day period band is present in all experiments. The experiments (not shown) were repeated for the boundary condition moved to 50 W, as in the modified control run (Fig. 4b), but little difference was found.

Collectively, Experiments 1–3 point to a rather clear conclusion. The state of transients in the eastern Pacific Ocean appears to be independent of the variability of the eastern boundary conditions of the domain. That is, disturbances in the eastern Pacific quite likely arise from in situ processes. Finally, there appears to be no essential difference between Experiment 3 and 4 indicating that the orography of Central America and southern Mexico has little impact on the generation of disturbances in the eastern Pacific Ocean.

The latitude-height structure of the mean meridional circulations of Experiments 2–4 is presented in Fig. 8. The results do not differ significantly from either the observations or the control cases shown in Fig. 3c. Each section has low-level cross-equatorial flow and a stronger return flow. In all of the three sections, there is a low-level divergence doublet bisected by zero absolute vorticity contour. Also, in each case there is evidence of the shallow mid-level meridional. In all three instances, the $\eta = 0$ contour, from surface to about 500 hPa, is located north of the equator, suggesting an inertially unstable regime. There are differences, of course, such as the stronger upper and lower meridional flow in Experiment 3. But the form of the circulations is very similar to what is expected of an inertially unstable regime as described in Part I.

5 Conclusions

In Part I of this study, it was suggested that the location of mean convection and the higher-frequency variance of the ITCZ were the result of local dynamical processes. An important corollary is that the majority of easterly waves in the Pacific Ocean develop in situ rather than propagate from the western Atlantic Ocean. Despite a degree of consistency between observations and theoretical expectations, the arguments made in Part I require further substantiation, as other hypotheses are possible. The propagation of waves from the Atlantic to the Pacific needs to be revisited. Also, it has been suggested that the impact of the near-equatorial mountain ranges of Central America and Southern Mexico render the eastern Pacific unstable. To test this range of alternative solutions, a series of experiments were designed using the WRF regional model. The initial and boundary conditions were set to include westward propagating disturbances from the Atlantic Ocean, in the first instance (Experiment 1), and then exclude them in a second instance (Experiments 2 and 3). Both sets of results, with and without disturbances at the eastern boundary, provide a simulation of the basic structure of the ITCZ, oscillations of a time scale similar to the inertial frequency of the mean location of ITCZ convection, and the generation of westward propagating waves, again with the same inertial frequency. Finally, the impact of orography was shown to be minimal. In Experiment 4, where orography is flattened, there was little difference in the structure of the response compared to any of the other experiments.

In conclusion, numerical experimentation corroborates the diagnostic and theoretical conclusions of Toma and Webster (2008) that local instabilities associated with the strong CEPG in the eastern Pacific Ocean promote in situ development of easterly waves. In each of the experiments, the only common denominator was the strong CEPG.

Acknowledgments This research was conducted with funding provided by the Climate Dynamics Division of the National Science Foundation under award NSF-ATM 0531771. Partial funding of Dr. Toma came from the NOAA CPPA project NA060OAR4310005. We are indebted to Drs. Carlos Hoyos and Paula Agudelo for many fruitful discussions.

References

Adler SGRF, Huffman GJ, Chang A, Ferraro R, Xie P, Janowiak J, Rudolf B, Schneider U, Curtis S, Bolvin D, Gruber A, Susskind J, Arkin P (2003) The version 2 Global Precipitation Climatology Project (GPCP) monthly precipitation analysis (1979–present). J Hydrometeorol 4:1147–1167. doi: 10.1175/1525-7541(2003)004<1147:TVGPCP>2.0.CO;2

Betts AK, Miller MJ (1993) The Betts–Miller scheme. The representation of cumulus convection in numerical models. Meteor Monogr Amer Meteor Soc 46:107–121

Dudia J (1989) Numerical study of convection observed during the winter monsoon experiment using a mesoscale two-dimensional model. J Atmos Sci 46:3077–3107. doi: 10.1175/1520-0469(1989)046<3077:NSOCOD>2.0.CO;2

Farfan LM, Zehnder JA (1997) Orographic influence on the synoptic-scale circulations associated with the genesis of Hurricane Guillermo (1991). Mon Weather Rev 125:2683–2698. doi: 10.1175/1520-0493(1997)125<2683:OIOTSS>2.0.CO;2

Hodges KI, Hoskins BJ, Boyle J, Thorncroft J (2003) A comparison of recent reanalysis datasets using objective feature tracking:

storm tracks and tropical easterly waves. Mon Weather Rev 131:2012–2037. doi: 10.1175/1520-0493(2003)131<2012:ACORRD>2.0.CO;2

Hong S-Y, Dudhia J, Chen S-H (2004) A revised approach to ice-microphysical processes for the bulk parameterization of cloud and precipitation. Mon Weather Rev 132:103–120. doi: 10.1175/1520-0493(2004)132<0103:ARATIM>2.0.CO;2

Janjic ZI (1994) The step-mountain Eta coordinate model: further developments of the convection, viscous sublayer, and turbulence closure schemes. Mon Weather Rev 122:927–945. doi: 10.1175/1520-0493(1994)122<0927:TSMECM>2.0.CO;2

Kerns B, Greene K, Zipser E (2008) Four years of tropical ERA-40 vorticity maxima tracks. Part I: climatology and vertical vorticity structure. Mon Weather Rev 136:4301–4319. doi: 10.1175/2008MWR2390.1

Laprise R (1992) The Euler equations of motion with hydrostatic-pressure as an in dependent variable. Mon Weather Rev 120:197–208. doi: 10.1175/1520-0493(1992)120<0197:TEEOMW>2.0.CO;2

Mlawer EJ, Taubman SJ, Brown PD, Iacono MJ, Clough SA (1997) Radiative transfer for inhomogeneous atmospheres: RRTM, a validated correlated-k model for the longwave. J Geophys Res 102(16):663–682

Noh Y, Cheon W-G, Hong S-Y (2003) Improvement of the K-proÞle model for the planetary boundary layer based on large eddy simulation data. Boundary Layer Meteorol 107:401–427. doi: 10.1023/A:1022146015946

Raymond DJ, Bretherton CS, Molinari J (2006) Dynamics of the intertropical convergence zone of the East Paciþc. J Atmos Sci 63:582–597. doi: 10.1175/JAS3642.1

Reynolds RW, Rayner NA, Smith TM, Stokes DC, Wang WQ (2002) An improved in situ and satellite SST analysis for climate. J Clim 15:1609–1625. doi: 10.1175/1520-0442(2002)015<1609:AIISAS>2.0.CO;2

Serra YL, Kiladis GN, Cronin MF (2008) Horizontal and vertical structure of easterly waves in the Paciþc ITCZ. J Atmos Sci 65:1266–1284. doi: 10.1175/2007JAS2341.1

Skamarock WC, Klemp JB, Dudhia J, Gill DO, Barker DM, Wang W, Powers JG (2005) A description of the advanced research WRF version 2. NCAR Technical Note, NCAR/TN-468

Toma VE, Webster PJ (2008) Oscillations of the Intertropical Convergence Zone and the genesis of easterly waves. Part I diagnostics theory (submitted to). Clim Dyn

Tomas R, Webster PJ (1997) On the location of the Intertropical Convergence zone and near-equatorial convection: The role of inertial instability. Q J R Meteor Soc 123:1445–1482. doi: 10.1002/qj.49712354202

Tomas RA, Holton JR, Webster PJ (1999) The inßuence of cross-equatorial pressure gradients on the location of near-equatorial convection. Q J R Meteor Soc 125:1107–1127. doi: 10.1256/smsqj.55602

Uppala SM, Kållberg PW, Simmons AJ, Andrae U, da Costa Bechtold V, Fiorino M, Gibson JK, Haseler J, Hernandez A, Kelly GA et al (2005) The ERA-40 reanalysis. Q J R Meteor Soc 131:2961–3012. doi: 10.1256/qj.04.176

Wicker LJ, Skamarock WC (2002) Time-splitting methods for elastic models using forward time schemes. Mon Weather Rev 130:2088–2097. doi: 10.1175/1520-0493(2002)130<2088:TSMFEM>2.0.CO;2

Zehnder JA, Gall RL (1991) Alternative mechanisms of tropical cyclone formation in the Eastern North Paciþc. Atmosfera 4:5–37

Zehnder JA, Powell DM, Ropp DL (1999) The interaction of easterly waves, orography, and the intertropical convergence zone in the genesis of eastern paciþc tropical cyclones. Mon Weather Rev 127:1566–1585. doi: 10.1175/1520-0493(1999)127<1566:TIOEWO>2.0.CO;2

Zhang C, McGauley M, Bond NA (2004) Shallow meridional circulation in the tropical eastern Paciþc. J Clim 17:133–139. doi: 10.1175/1520-0442(2004)017<0133:SMCITT>2.0.CO;2